machines

MDPI

Article

Coal–Rock Cutting Sound Denoising Based on Complete Ensemble Empirical Mode Decomposition with Adaptive Noise and an improved Fruit Fly Optimization Algorithm

Chaofan Ren [1], Jing Xu [1,2,*], Jie Xu [1], Yanxin Liu [1] and Ning Sun [1]

[1] School of Mechanical Engineering, Jiangsu University of Science and Technology, No.666 Changhui Road, Zhenjiang 212114, China; rcf666888@163.com (C.R.); xujie9js@163.com (J.X.); lyanxin1998@163.com (Y.L.); 15262132649@163.com (N.S.)

[2] Marine Equipment and Technology Institute, Jiangsu University of Science and Technology, No.2 Mengxi Road, Zhenjiang 212008, China

* Correspondence: xujing@just.edu.cn; Tel./Fax: +86-511-8889-2131

Abstract: The cutting sound signal of a coal mining shearer is an important signal source for identifying the coal–rock cutting mode and load state. However, the coal–rock cutting sound signal directly collected from the industrial field always contains a large amount of background noise, which is not conducive to the subsequent feature extraction and recognition. Therefore, efficient noise elimination for the original signal is required. An intelligent processing method based on an improved complete ensemble empirical mode decomposition with adaptive noise (CEEMDAN) denoising algorithm is constructed for the cutting sound signal in this paper. CEEMDAN first decomposes the sound to generate a series of intrinsic modal functions (IMFs). Because the denoising threshold of each IMF is usually obtained by an experimental test or an empirical formula in the traditional CEEMDAN method, obtaining an optimal threshold set for each IMF is difficult. The processing effect is often restricted. To overcome this problem, the fruit fly optimization algorithm (FOA) was introduced for CEEMDAN threshold determination. Moreover, in the basic FOA, the scouting bee mutation operation and adaptive dynamic adjustment search strategy are applied to maintain the convergence speed and global search ability. The simulation result shows that the signal waveform processed by the improved CEEMDAN denoising algorithm is smoother than the other four typical eliminate noise signal algorithms. The output signal's signal-to-noise ratio and mean square error are significantly improved. Finally, an industrial application of a shearer in a coal mining working face is performed to demonstrate the practical effect.

Keywords: coal–rock cutting sound signal; complete ensemble empirical mode decomposition with adaptive noise; fruit fly optimization algorithm; scouting bee mutation; adaptive dynamic adjustment search

check for updates

Citation: Ren, C.; Xu, J.; Xu, J.; Liu, Y.; Sun, N. Coal–Rock Cutting Sound Denoising Based on Complete Ensemble Empirical Mode Decomposition with Adaptive Noise and an improved Fruit Fly Optimization Algorithm. *Machines* **2022**, *10*, 412. https://doi.org/10.3390/machines10060412

Academic Editor: Hélène Chanal

Received: 7 April 2022
Accepted: 5 May 2022
Published: 25 May 2022

Publisher's Note: MDPI stays neutral with regard to jurisdictional claims in published maps and institutional affiliations.

Copyright: © 2022 by the authors. Licensee MDPI, Basel, Switzerland. This article is an open access article distributed under the terms and conditions of the Creative Commons Attribution (CC BY) license (https://creativecommons.org/licenses/by/4.0/).

1. Introduction

The shearer is one of the key pieces of equipment in the comprehensive mechanized coal mining face. The cutting sound signal generated by the shearer's colliding drum with coal and rock contains a lot of key information during its operation. This information can represent the shearer's current cutting state and load condition. By excavating the cutting sound signal, the load condition and fault information of the shearer could be recognized. In recent years, shearer cutting state identification based on the sound signal has gained the attention of scholars [1–3]. However, there are many sources of sound in coal mining faces. The original sound signals collected on-site are mixed signals from multiple sound sources and cannot be used directly. How to remove the noise signal from the complex mixed sound signal to the maximum extent and retain the coal and rock cutting signal is extremely important for subsequent feature extraction and recognition.

Preliminary research shows that the coal–rock cutting sound signal has the characteristics of being nonperiodic, nonstationary, and discontinuous [4]. Traditional denoising algorithms based on fast Fourier transform, wavelet transform, and wavelet packet transform are difficult to achieve effectively, removing noise components when processing such signals [5,6]. Empirical mode decomposition (EMD), which does not require selecting the basis function and decomposition layer, can adaptively decompose the signals according to different time scales when processing the signal and can extract the features of nonstationary signal variations [7]. Torre et al. proposed the complete ensemble empirical mode decomposition with adaptive noise (CEEMDAN) based on EMD [8]. In CEEMDAN, Gaussian white noise is adaptively added to each order of intrinsic mode function (IMF) component, and then superimposed and canceled. In this way, the reconstruction error caused by adding noise will be eliminated in the decomposition iteration. It not only guarantees the accuracy of signal decomposition but also effectively avoids the modal blending in the traditional EMD decomposition process [9]. Therefore, signal processing accuracy and completeness are improved.

The signal denoising method based on CEEMDAN is to decompose the signal into several components, and then shrink and transform the components in each order to eliminate the noise components in the mixed signals. Peng and others denoised the original signal through CEEMDAN and filtering algorithms and obtained certain results [10]. A joint noise elimination method based on CEEMDAN and a nonlocal mean algorithm was proposed by Zhang and others. Finally, the feasibility and applicability of this method for signal noise reduction in practical engineering are verified [11]. The lifting wavelet transform technique and the CEEMDAN method were combined in reference [12] to improve the computational efficiency and signal reconstruction accuracy and realize the denoising of fiber optic gyroscope signals. A denoising method based on CEEMDAN, least mean square difference criterion, and a least mean square adaptive filter were proposed by Li-y and others. By analyzing the simulation signal and the real underwater acoustic signal, the method was proved to have a better denoising effect [13].

The above studies investigated and applied the CEEMDAN-based denoising algorithm, achieving certain results. However, the determination of each order of IMF denoising thresholds is mostly obtained through comparative experiments or empirical formulas, which requires a significant amount of calculation. It is difficult to obtain the best denoising effect in the face of randomly varying noisy signals [14]. In recent years, with the widespread use of artificial intelligence, adaptive threshold selection methods based on intelligent optimization algorithms have been gradually adopted. In [15], the CEEMDAN threshold was modified by a niche genetic algorithm, and an application example on ECG signals was shown to verify the effectiveness of the proposed work. A hybrid wind energy prediction model based on CEEMDAN, SVD, and PSO was presented by Zhang and others. The final prediction results showed that the proposed model can improve the effect of wind speed prediction, reduce the prediction error, and provide strong support for the stable operation of wind farms, and the grid connection of power plants [16].

The fruit fly optimization algorithm (FOA) is a new biological intelligent optimization algorithm proposed by Pan in 2012. FOA, as a meta-heuristic method, simulates the foraging behavior of fruit fly individuals and groups, flies in the direction of the highest food concentration, and conducts appropriate iterations to find the global optimal solution [17]. The fruit fly is spatially and visually superior to other species. It can even sniff out food sources up to 40 km away and identify aggregations of other animals through its sensitive vision [18]. Compared with the abovementioned optimization algorithms, FOA has the advantages of a simple structure, fewer setup parameters, direct applicability to practical applications, easy implementation, and fast convergence. Since FOA was proposed, it has been widely applied in time series prediction [19], neural network parameter optimization [20], task cooperative planning [21], and other fields. FOA has a strong convergence speed and the ability to deal with optimization problems. However, it is single in diversity and does not have a high probability of mutation. As a result, the search

space will be limited. When the global optimal is shifted away from an overly converged swarm, it is difficult for FOA to jump away from the local extremum, and diversity is lost. To improve the performance of the basic FOA and avoid local optimization, certain modified approaches were proposed to strengthen the local and global optimal values. In [22], the back-propagation neural network based on an improved fruit FOA (IFOA-BP) was applied to load forecasting. The simulation results showed that the algorithm can improve the prediction accuracy of wind energy and load. Guo and others introduced two concepts, sensitivity, and pheromone, which improve the optimization strategy and position replacement of fruit flies and modify the global optimization characteristics of the algorithm. The experimental results showed that the model's minimum prediction error accuracy is only 0.55%, indicating a more robust prediction effect [23]. Furthermore, an olfactory search and a visual search were adopted in FOA to effectively solve the inverse kinematics problem of redundant manipulators [24]. Many improvements focusing on the FOA have been elaborated in recent years, but few researchers have been able to balance both local extremes and iterative rates.

To remove noise components from the original coal–rock cutting sound signal, an adaptive threshold noise elimination method based on improved CEEMDAN is proposed in this paper. To overcome the difficulty of determining the optimal denoising threshold for each order of IMF in the traditional CEEMDAN denoising, FOA iterative convergence has been introduced to perform global optimization for each order of the IMF threshold. At the same time, it is easy to fall into a local optimum in the iterative process to avoid the simple diversity of the FOA population. In an artificial bee colony (ABC), the mutation mode of scouting bees is combined with FOA to divide the fruit flies into the native and mutation groups separately. Furthermore, the adaptive dynamic adjustment search strategy is introduced to flexibly generate the range of variation population and improve the convergence accuracy and maintain the convergence speed. The rest of the paper is organized as follows: In Section 2, the basic principles of CEEMDAN and FOA are first introduced. Section 3 introduces the improvement of FOA and the improved CEEMDAN adaptive denoising method and optimization process. In Section 4, to verify the effectiveness and superiority of the proposed method, Gaussian white noise with a different SNR is added to the simulation signal, and different denoising algorithms are compared and verified using simulation. In Section 5, the improved CEEMDAN denoising algorithm is used to denoise the shearer coal–rock cutting sound signal, and a joint time-frequency domain analysis is performed to verify the practical application effect. Some conclusions and outlooks are summarized in Section 6.

2. Basic Theory

2.1. CEEMDAN Denoising Algorithm

CEEMDAN adaptively added several pairs of positive and negative Gaussian white noise according to the signal characteristics, decomposed the first layer of IMF components, and immediately calculated the average to get the first IMF. The above operations continue for the residual signal $R(t)$ until the decomposition ends when the residual signal $R(t)$ is a monotone function. Each stage is selected by calculating a signal-to-noise control factor to add positive and negative Gaussian white noise with different signal-to-noise ratios [25]. Each order of IMF must satisfy the following two conditions: in the whole time range, the difference between the number of zeros and extreme points in the function is not more than one; the average value of the upper and lower envelope, composed of local maxima and local minima, is zero at any point. CEEMDAN effectively solves the problem that the EMD decomposition process is prone to modal aliasing and improves the completeness, decomposition efficiency, and reconstruction accuracy of the decomposition process [26]. Finally, the original signal $x(t)$ can be expressed as:

$$x(t) = R(t) + \sum_{k=1}^{k} IMF_k(t) \quad (1)$$

CEEMDAN is a linear transformation. The coefficients of the decomposed noisy signal include the noise signal coefficient and the useful signal coefficient. CEEMDAN denoising is similar to the principle of wavelet denoising, and the threshold of each order IMF should be determined [27]:

$$T_i = C\sqrt{E_i 2\ln^N} \tag{2}$$

where T_i denotes the threshold for the i-th IMF, C is a constant between [0, 1], N is the signal data length, and E_i is the estimated energy of the first IMF.

$$E_i = \frac{E_1}{\alpha}\beta^{-i} \tag{3}$$

where E_i is the variance of the first IMF and α and β are constants determined by a large number of independent experiments or empirical formulas.

Unlike wavelet threshold denoising, CEEMDAN uses intermittent threshold denoising. For each IMF with a random neighboring zero interval $z_{i,j} = [z_{i,j}, z_{i,j+1}]$, a hard threshold denoising function is defined within the interval:

$$h_i^g(z_{i,j}) = \begin{cases} h_i(z_{i,j}) & \left|h_i(r_{i,j})\right| > T_i \\ 0 & \left|h_i(r_{i,j})\right| \le T_i \end{cases} \tag{4}$$

Additionally, the soft threshold denoising function is defined in the interval:

$$h_i^g(z_{i,j}) = \begin{cases} \mathrm{sgn}(h_i(z_{i,j}))\left(\left|h_{i,j}\right| - T_i\right) & \left|h_i(r_{i,j})\right| > T_i \\ 0 & \left|h_i(r_{i,j})\right| \le T_i \end{cases} \tag{5}$$

where $h_i(r_{i,j})$ is the maximum value in the interval and $h_i(r_{i,j})$ is the data point in $[z_{i,j}, z_{i,j+1}]$.

The final denoised signal is expressed as:

$$x^g(t) = R(t) + \sum_{i=1}^{k} h_i^g(t) \tag{6}$$

where $x^g(t)$ is the denoised signal.

The CEEMDAN denoising process reveals that the selection of the soft and hard thresholding functions and the threshold values of each order are important factors influencing the denoising effect. The hard threshold function denoising signal is discontinuous, resulting in a vibration phenomenon [28]. The signal is still a continuous signal with a high degree of signal reduction after the soft threshold function denoising. In practice, soft threshold function denoising is mostly used [29]. For each order denoising threshold, if the threshold is chosen too small, it will lead to incomplete denoising; if the threshold is chosen too high, the detailed information of the signal will be easily ignored. Currently, the denoising thresholds for each order of IMF are primarily determined by simulation cross-comparison experiments or empirical formulas, which requires a significant amount of work and makes obtaining the optimal denoising threshold difficult.

2.2. Fruit Fly Optimization Algorithm

The fruit FOA is a new biological intelligent optimization algorithm proposed by Pan in 2012. By simulating the foraging behavior of fruit flies as individuals and groups, they fly in the direction of the highest food concentration and conduct appropriate iterations to find the global optimal solution [17]. During the foraging process, information about the location of food is constantly exchanged between individuals so that the whole group can quickly follow the shortest path to find food. FOA has the advantages of simple structure, few setting parameters, direct application, easy implementation, and fast convergence. Since FOA was proposed, it has been widely applied in time series prediction, neural

network parameter optimization, task cooperative planning, and other fields. The FOA optimization process is as follows:

(1) Several key parameters of the fruit FOA are determined: population size P, maximum iteration N, search range LR, flight distance FR, and the initialization of the population locations.

$$\begin{aligned} X_{axis} &= LR \times rand(\cdot) \\ Y_{axis} &= LR \times rand(\cdot) \end{aligned} \tag{7}$$

where $rand(\cdot)$ is a random function that follows a uniform distribution.

(2) Using the sense of smell, the direction and distance of each fruit fly in the population are determined.

$$\begin{aligned} X_i &= X_{axis} + FR \times rand(\cdot) \\ Y_i &= Y_{axis} + FR \times rand(\cdot) \end{aligned} \tag{8}$$

where $i = 1, 2, 3, \ldots P$, (X_i, Y_i) is the position of the i-th fruit fly.

(3) After the location of each fruit fly in the population is determined, the distance $Dist_i$ of each fruit fly to the origin is determined, and the reciprocal of $Dist_i$ represents the judgment value of taste concentration at this location.

$$\begin{aligned} Dist_i &= \sqrt{x_i^2 + y_i^2} \\ S_i &= 1/Dist_i \end{aligned} \tag{9}$$

(4) $Smell_i$ is solved by S_i and $Function$. The optimal odor concentration for each fruit fly in the population is determined.

$$\begin{aligned} Smell_i &= Funtion(S_i) \\ [bestsmell\ bestindex] &= \max(smell) \end{aligned} \tag{10}$$

(5) The location of the best flavor concentration causes the rest of the population to fly toward that point.

$$\begin{aligned} &Smellbest = bestsmell \\ &\begin{cases} X_{axis} = X_{bestindex} \\ Y_{axis} = Y_{bestindex} \end{cases} \end{aligned} \tag{11}$$

where $(X_{bestindex}, Y_{bestindex})$ is the individual position of a drosophila corresponding to its fitness value $bestindex$.

(6) Steps 2-5 are repeated for iterative optimization. The flavor concentrations obtained from each iteration are compared until the end of the iteration, when the global optimum solution is obtained. The process of fruit fly group foraging behavior is shown in Figure 1 [30].

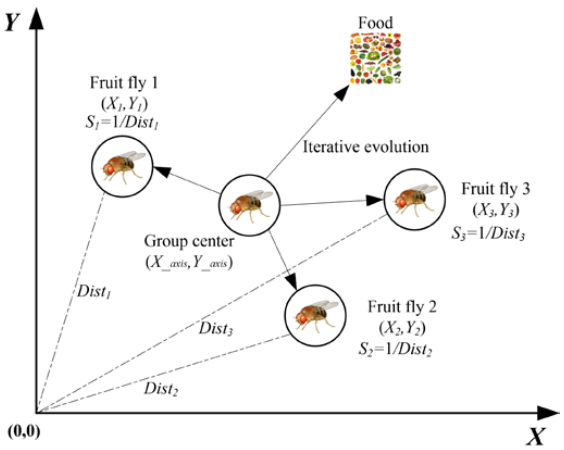


Figure 1. Process of foraging behavior for a fruit fly group.

3. The Proposed Method

3.1. Improvement of FOA

The steps of the original FOA in searching for the optimal solution will reveal that it is single in diversity and does not have a high probability of mutation. Hence, the search space will be limited. When the global optimal is shifted away from a too converged swarm, it is difficult for FOA to jump away from the local extremum, and diversity is lost.

The ABC has the advantages of simple calculation, fast convergence speed, and strong global optimization ability [31]. ABC's ability to jump out of the locally optimal solution is dependent on the scout bee's mutation role. During the search, if the nectar source has not been updated to a better nectar source after n iterations and reaches the optimal solution not updated the number of times L, the nectar source will be abandoned. Scouting bees will go out and randomly generate a new nectar source. To balance the ability of global and local search, some improvements to the original FOA are pointed out in this paper. Scouting bees' mutation method and FOA combined to increase the diversity of the population. In this way, while retaining the local search ability of the original FOA, the global optimization expansion ability of the population is improved, and the convergence ability of the population is maintained. In this case, the optimal solution is not updated. The number of times L is determined by the object applied by the algorithm. If the value is too large, the algorithm will have little improvement; if the value is too small, the local search ability will be weakened. The value of L needs to be determined according to the specific situation. Based on empirical values, L is set as the product of population size and problem dimension [32].

In addition, considering that the optimal fitness value may appear near the local optimal concentration value S_i, it is also considered to further expand the search scope, jump out of the local optimal concentration value S_i, and improve the convergence rate. Therefore, the adaptive dynamic adjustment search strategy is introduced, and the population position mutation range S_i' is set as $[S_i \pm 2]$. The principle of the mutation is presented in Figure 2. The mutation population has the same number of individuals as the basic population. The flowchart of the IFOA can be shown in Figure 3.

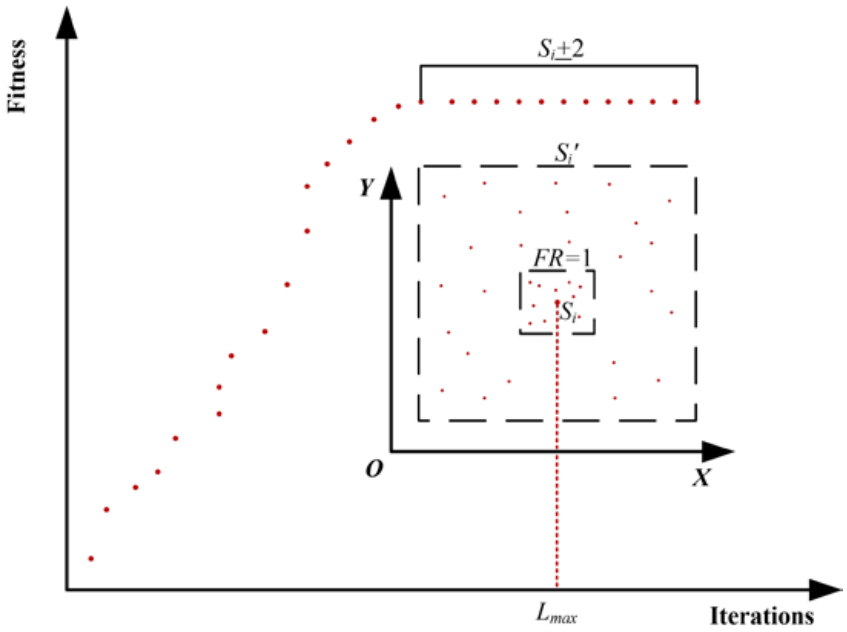


Figure 2. Flowchart of the IFOA.

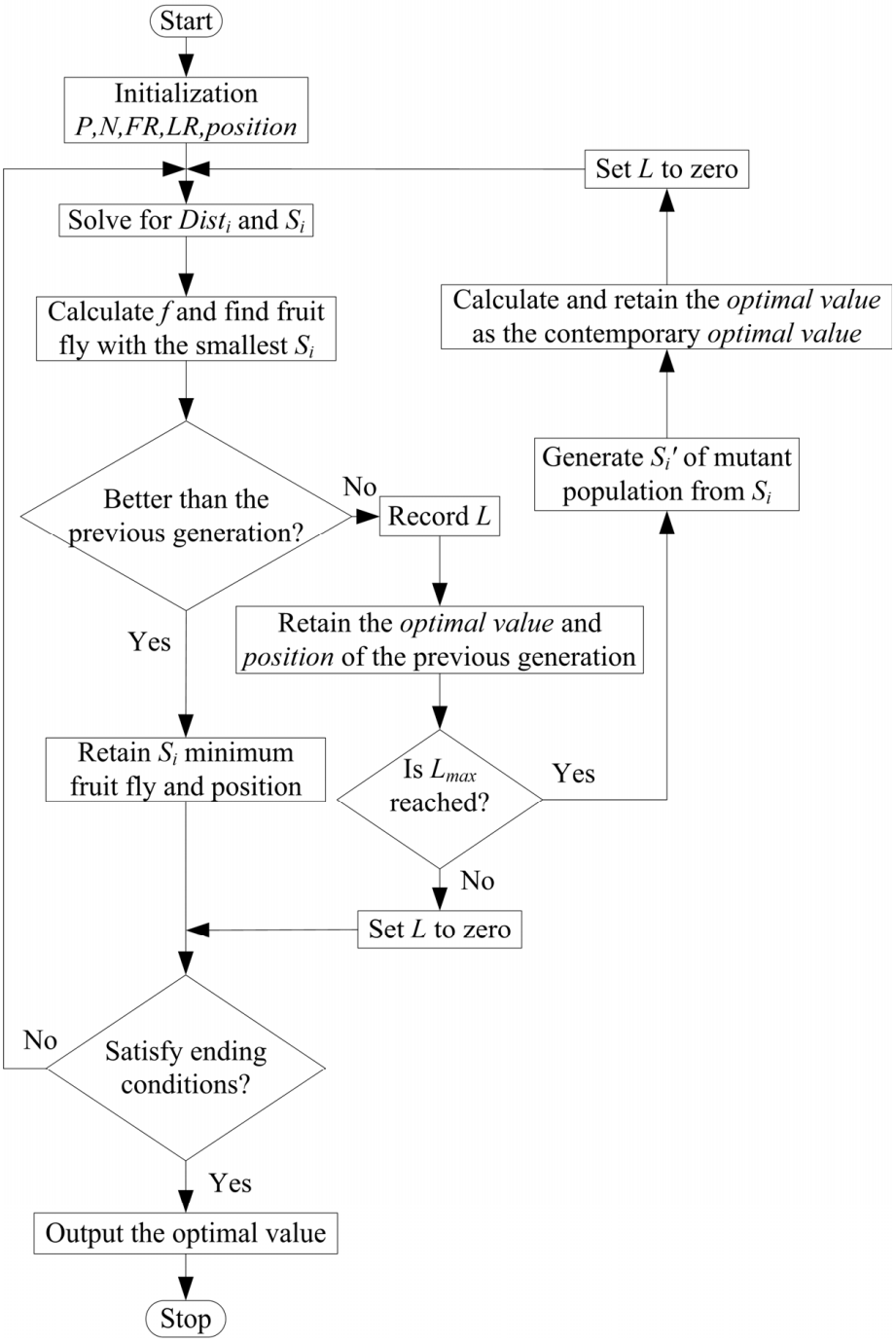


Figure 3. Flowchart of the IFOA.

3.2. Flow of the Proposed Denoising Method

To obtain the best denoising effect of CEEMDAN, this paper uses IFOA adaptive seeking to obtain the best denoising threshold for each order of IMF and proposes an adaptive denoising algorithm based on the improved CEEMDAN. The main process of the algorithm is as follows:

Step 1: The parameters of the improved CEEMDAN are initialized, such as P, LR, N, FR, L, and the number of populations K. Positions of each fruit fly population, as well as the flight direction and distance of individuals in each fruit fly population are initialized. In the improved CEEMDAN denoising algorithm, each order IMF threshold is optimized by a fruit fly population.

Step 2: CEEMDAN decomposition is performed on the coal–rock cutting sound signal containing noise to obtain each order of IMF. The distance of each fruit fly individual to the origin $Dist_i$ and the flavor concentration judgment value S_i are calculated. Each S_i corresponds to a g_i, which is a threshold feasible solution, so there are P^N combinations of threshold feasible solutions.

A wider range of soft threshold functions are used for denoising in this paper, and each set of feasible solutions is used for threshold denoising of each order of IMF. Using the constructed fitness function fit, the fitness values under the feasible solutions corresponding to each IMF threshold are calculated. The maximum value *Smellbest* and the corresponding optimal threshold $Smell_g$ are recorded, updating each population position and the corresponding position of each fruit fly individual. The fitness evaluation function fit constructed by the signal independence theory is as follows:

$$fit = \frac{1}{1+g^2} \tag{12}$$

$$g = \frac{[r_{22} \times hr_{21}]^2}{r_{11}^2} \tag{13}$$

where r_{22} is the autocorrelation of noise. Its rising value means that more of the original signal is attached to the noise, so the reconstructed signal will not recover well. hr_{21} is the high order cross-correlation between useful signal and noise. Its decline means that the two signals have become more independent. Therefore, the original signal and noise gradually separate. r_{11} is the autocorrelation of useful signals. An ascending value implies that its component is more than a component of noise. Hence, the restructured signal has a good recovery [33,34]. r_{22}, hr_{21}, r_{11} are defined as follows:

$$r_{ij} = \frac{C_{ij}}{\sqrt{C_{ii}C_{jj}}} = \frac{\mathrm{cov}[s_i, s_j]}{\sqrt{\mathrm{cov}[s_i]\mathrm{cov}[s_j]}}, i, j = 1, 2 \tag{14}$$

$$hr_{ij} = \frac{HC_{ij}}{\sqrt{HC_{ii}C_{jj}}} = \frac{\mathrm{cov}[\varphi(s_i), s_j]}{\sqrt{\mathrm{cov}[\varphi(s_i)]\mathrm{cov}[s_j]}}, i, j = 1, 2 \tag{15}$$

where s_1 is the useful signal, s_2 is the noise component, $\mathrm{cov}[s_i, s_j] = E\{[s_i - E(s_i)][s_j - E(s_j)]\}$, $\mathrm{cov}[s_i] = E\{[s_i - E(s_i)]^2\}$, $E(s_i)$ is the mathematical expectation of s_i and $\varphi(s_i) = s_i^2 + s_i^3.r_{22}$ and hr_{21} tend to the minimum and r_{11} tends to the maximum when the location of each fruit fly group is placed in the best. Then, g is the minimal and fit is the maximal [35].

Step 3: The fitness value under the feasible solution of each IMF threshold in each combination is calculated, and the maximum fitness value is recorded as *bestsmell*. The global maximum value *Smellbest* is compared with the current maximum value *bestsmell*. If the global maximum value is smaller than the current maximum value, *bestsmell* is used to replace *Smellbest*, and the current optimal threshold value $best_g$ is used to replace $Smell_g$, and the location of each fruit fly population is updated.

Step 4: Judge whether the iteration number n reaches the maximum iteration number N or the error meets the preset accuracy. If not, proceed with Step 2-Step 3. If so, iteration is stopped. The CEEMDAN reconstruction is carried out, and a shearer coal-rock cutting sound signal corresponding to each IMF under optimal threshold denoising is output. The flowchart of the process can be shown in Figure 4.

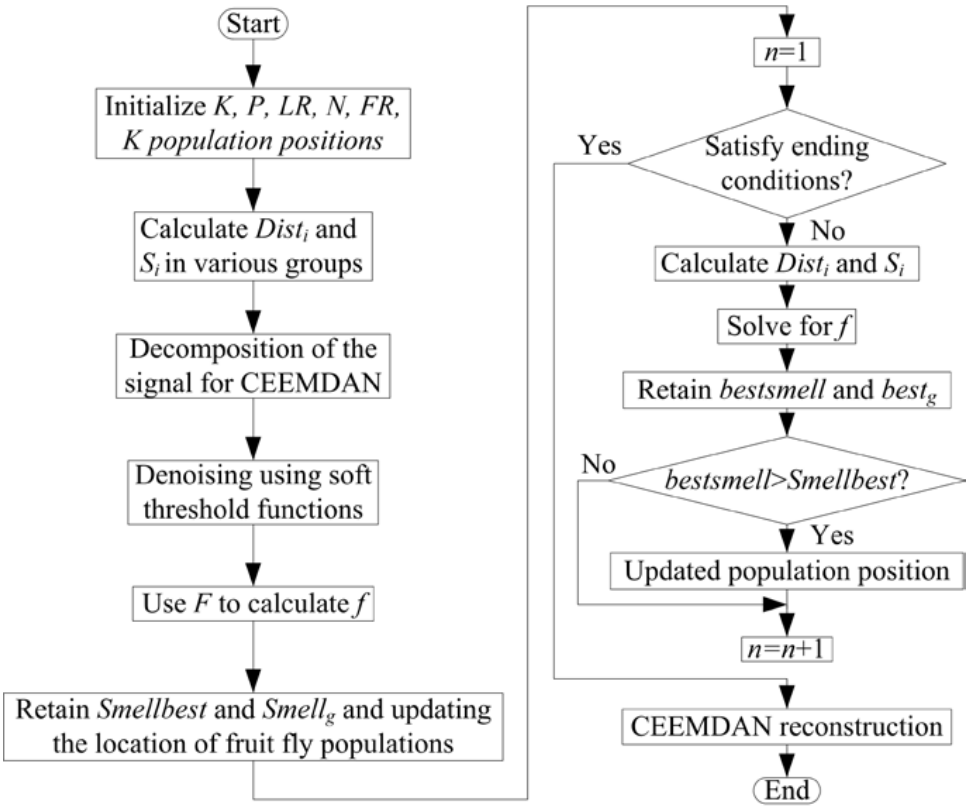


Figure 4. Based on the improved CEEMDAN coal–rock cutting sound signal denoising process.

4. Simulation

4.1. Experimental Data and Evaluation Indicators

The denoising algorithm was tested by combining simulation with engineering experiments to verify its feasibility and effectiveness. The simulation environment of this paper is the Matlab2020 software platform, built on the Windows 10 system. A piece of the pure train sound signal from the Matlab2020 sptool toolbox is extracted with a sampling frequency of 8192 Hz and data length of 12,880. White Gaussian noise with input SNR (SNR_{in}) of 0 dB, 10 dB, 20 dB, and 30 dB was added to the pure sound signal, respectively. The original signal and the noisy signal were shown in Figure 5. It can be seen from the waveform of the original signal that the amplitude of the signal varied widely in the time domain, and there were two obvious ups and downs. The first amplitude rose and fell rapidly, while the second rose and fell relatively slowly. In addition, with the decrease in SNR_{in}, the waveform of the original signal was gradually submerged. Taking SRN_{in} = 10 dB as an example, the CEEMDAN decomposition of the noise-containing signal was then performed to obtain each order of IMF components and the residual signal as shown in Figure 6. The decomposed signal can be expressed as X = IMF1 + IMF2 + IMF3 + … + IMF14 + RES, which corresponds to Formula (1). It can be seen that each IMF component had no mode aliasing phenomenon and the noise was mainly distributed in the high-frequency inherent component.

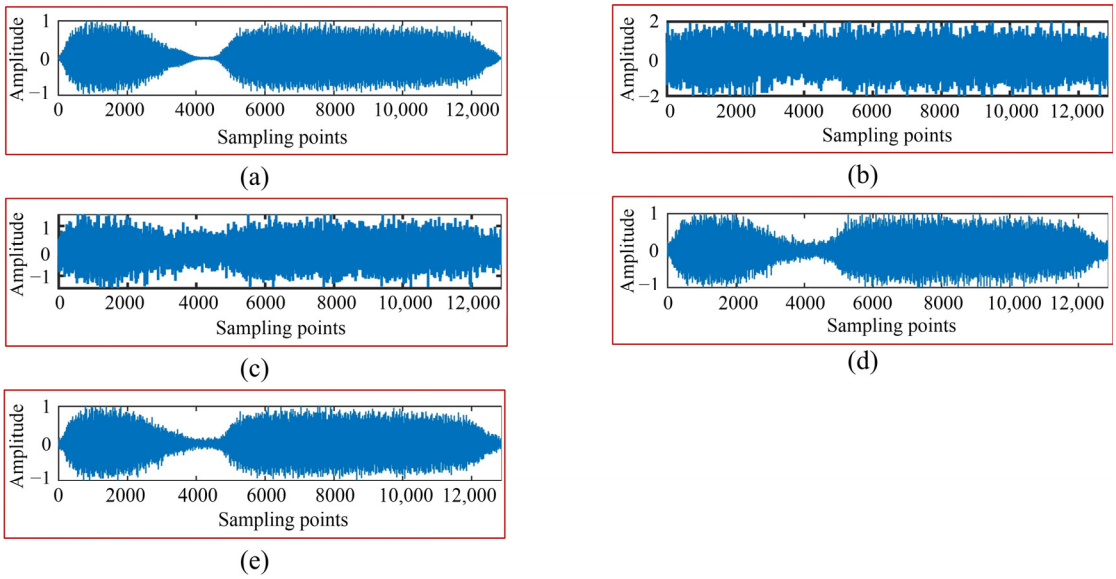


Figure 5. (**a**) Original sound signal; (**b**) SNR_{in} = 0 dB noisy sound signal; (**c**) SNR_{in} = 10 dB noisy sound signal; (**d**) SNR_{in} = 20 dB noisy sound signal; (**e**) SNR_{in} = 30 dB noisy sound signal.

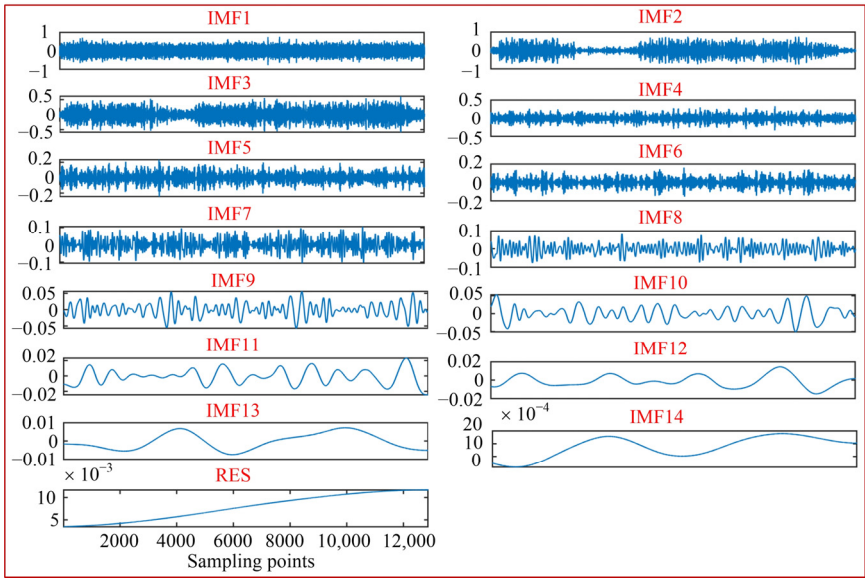


Figure 6. IMF components of each order with residual signal (SNR_{in} = 10 dB).

The signal-to-noise ratio of the output signal (SNR_{out}) and mean square error (MSE) were introduced as evaluation indexes to compare the denoising effects of the five algorithms intuitively. The larger the SNR and the lower the MSE after denoising, the greater the denoising effect will be. The formulas of SNR_{out} and MSE are as follows:

$$SNR_{out} = 10\lg\left(\sum_{t=1}^{N}(x(t)-s(t))^2 / \sum_{t=1}^{N}\left(\hat{x}(t)-s(t)\right)^2\right) \quad (16)$$

$$MSE = \frac{1}{N}\sum_{t=1}^{N}(s(t)-\hat{x}(t))^2 \quad (17)$$

where $x(t)$ is the noisy sound signal, $s(t)$ is the original pure signal, $\hat{x}(t)$ is the reconstructed sound signal, and N is the signal length.

4.2. Comparative Analysis

In this paper, EMD denoising, traditional CEEMDAN denoising, CEEMDAN-PSO denoising, CEEMDAN-FOA, and improved CEEMDAN denoising were, respectively, used to compare the denoising effects of the five algorithms. Among them, the EMD denoising and CEEMDAN denoising processes and parameter settings were referred to in the literature [36,37]. CEEMDAN-PSO denoising parameters refer to reference literature [38], set population size $P = 50$, self-learning factor $C_1 = 1.4$, group learning factor $C_2 = 1.4$, inertia weight $W = 0.8$, maximum iteration times $N = 300$, the number of populations $K = 14$. The CEEMDAN-FOA denoising algorithm sets the population size $P = 50$, the search range $LR = 10$, the maximum number of iterations $N = 300$, the flight distance $FR = 1$, and the number of populations $K = 14$. The improved CEEMDAN algorithm sets the population size $P = 50$, the search range $LR = 10$, the maximum number of iterations $N = 300$, the flight distance $FR = 1$, the number of populations $K = 14$, and the optimal solution without updating the number of times $L = 150$.

The processing results of the five denoising algorithms were shown in Figure 7. The signal waveform can show that the EMD denoising algorithms and CEEMDAN denoising algorithm had poor signal denoising effects, and the reconstructed signal differs significantly from the original pure sound signal in the waveform, with more burrs. CEEMDAN denoising was better than EMD denoising, but still contained a lot of noise. In contrast, the signal processed by the other three algorithms had a high degree of coincidence with the original signal, and the noise of the reconstructed signal after denoising was significantly reduced. It can be shown that the denoising threshold obtained using the intelligent optimization algorithm was more effective in denoising. The reconstructed signal waveform after improved CEEMDAN denoising was the smoothest of them all.

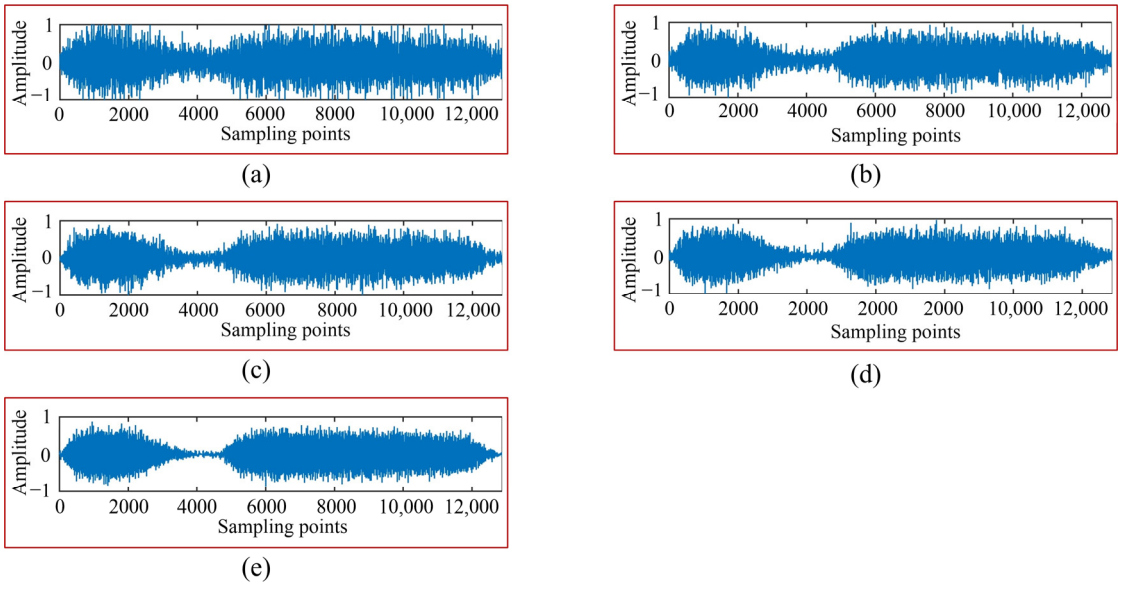


Figure 7. Five algorithms for denoising output waveform. (SNR_{in} = 10 dB). (**a**) EMD denoised output signal; (**b**) CEEMDAN denoised output signal; (**c**) CEEMDAN-PSO denoised output signal; (**d**) CEEMDAN-FOA denoised output signal; (**e**) Improved CEEMDAN denoised output signal.

In the case of different SNR_{in}, SNR_{out}, and *MSE*, they were shown in Table 1 after signal processing by five denoising algorithms. As can be seen from Table 1, with the decrease in the SNR_{in}, SNR_{out} gradually increases and *MSE* gradually decreases, indicating that the recovery degree of the denoising algorithm to the original signal was gradually enhanced. The improved CEEMDAN denoising algorithm showed that SNR_{out} and *MSE* were better than the other four algorithms in the case of four different SNR_{in}.

Table 1. SNR_{out} and *MSE* of different denoising methods.

SNR_{in}/ dB	Evaluation Indicators	EMD Denoising	CEEMDAN Denoising	CEEMDAN-PSO Denoising	CEEMDAN-FOA Denoising	Improved CEEMDAN Denoising
0	SNR_{out}	−48.0023	−46.5517	−45.1962	−44.6335	−44.0268
	MSE	0.7263	0.6965	0.6720	0.5076	0.4261
10	SNR_{out}	−46.5269	−44.3750	−43.2623	−42.5764	−42.0625
	MSE	0.6674	0.5823	0.5010	0.4881	0.3823
20	SNR_{out}	−45.1762	−43.2473	−42.6886	−41.3492	−41.1201
	MSE	0.5543	0.4892	0.3942	0.3118	0.3072
30	SNR_{out}	−45.0268	−43.0642	−42.5108	−41.1682	−41.0623
	MSE	0.5261	0.4631	0.3752	0.3479	0.3326

Under different SNR_{in}, compared with EMD denoising, CEEMDAN denoising, CEEMDAN-PSO denoising, and CEEMDAN-FOA denoising, the SNR_{out} of the proposed algorithm improved by 8.92%, 5.05%, 3.11%, and 1.29% on average, respectively, and the maximum increase was 9.60% (SNR_{in} = 10 dB), 5.42% (SNR_{in} = 0 dB), 3.67% (SNR_{in} = 20 dB), and 1.36% (SNR_{in} = 0 dB). The *MSE* and SNR_{out} had similar variation patterns. Compared with the four algorithms, MSE improved by 39.55%, 32.60%, 20.99%, and 12.19% on average, respectively, and the maximum improved by 42.71% (SNR_{in} = 10 dB), 38.82% (SNR_{in} = 0 dB), 37% (SNR_{in} = 0 dB), and 21.68% (SNR_{in} = 10 dB). This indicates that under different noise input conditions, the proposed algorithm can achieve better denoising effects compared with EMD denoising, CEEMDAN denoising, CEEMDAN-PSO denoising, and CEEMDAN-FOA denoising.

5. Industrial Application

The project team built an experimental platform for coal-rock cutting to denoise the sound signals collected on-site and compare the processing effects to further verify the effect of the algorithm proposed in this paper in practical engineering. The equipment layout and experimental site situation were shown in Figure 8.



Figure 8. (**a**) Experimental site equipment arrangement; (**b**) Experimental process of coal-rock cutting.

The sound sensor was installed on the rocker arm of the shearer facing the sample cutting and was fixed in the metal shell. The installed sound sensor belongs to the large diaphragm lateral acoustic-type external bias capacitive sensor. Shearer coal and rock cutting sound signals are similar to vibration, temperature, current, and other signals, all belonging to a one-dimensional signal sequence. The difference is that the characteristic frequencies of sound signals tend to be concentrated in the middle and high-frequency ranges (6.2016–8.9578 kHz and 11.7141–17.2266 kHz). According to the Nyquist sampling theorem, the sampling frequency of the sound sensor should be at least twice that of 20 kHz to avoid aliasing. To achieve better sampling, the sampling frequency of the sound sensor

was set to 44.1 kHz, and the maximum frequency component in the signal was 22.05 kHz, which can realize an omnidirectional direction. During the experiment, the sound sensor was installed on the shearer, and the sound signal collected at the front end was transmitted to the signal processing device through the MIC-IN interface. The shearer cutting operation is not only identified by the sound signal of coal and rock cutting caused by the collision between the drum and rock. It also includes the low-frequency area sound generated by the shearer's walking mechanism, the sound generated by the hydraulic heightening system, the sound generated by the operation of other equipment on-site, and the white noise distributed throughout the frequency and the impact noise with a random frequency distribution. Thus, the collected sound signals contained a lot of background noise, and the SNR of the shearer coal-rock cutting sound signal is low. It has an impact on the subsequent identification of coal and rock distribution states and shearer cutting states. The original signal was a piece of sound signal collected on-site. The improved CEEMDAN denoising algorithm proposed in this paper was used to carry out adaptive denoising of the original signal to improve the SNR of the shearer coal–rock cutting sound signal. To verify the method's effect on the signals, the characteristics of the time domain and frequency domain before and after denoising were analyzed. The original signal and the denoised signal were shown in Figure 9. The FFT was performed on the original signal and the denoised signal, and the characteristics of the frequency domain were shown in Figure 10. In addition, for the particularity of coal-rock cutting sound signal, a further study was made. The characteristics of the middle and high-frequencys domain of the coal-rock cutting sound signal before and after denoising were analyzed and compared. It was shown in Figure 11.

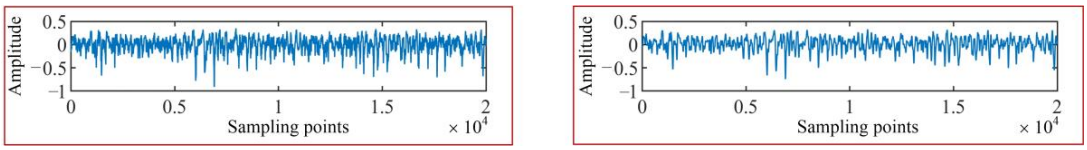


Figure 9. (**a**) Raw sound signals collected on-site; (**b**) Improved CEEMDAN denoised output signal.

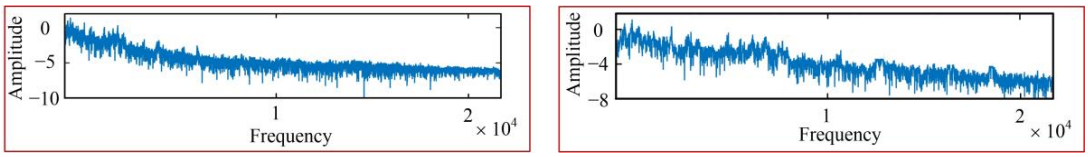


Figure 10. (**a**) Spectrogram of the original signal; (**b**) Spectrogram of the denoised signal.

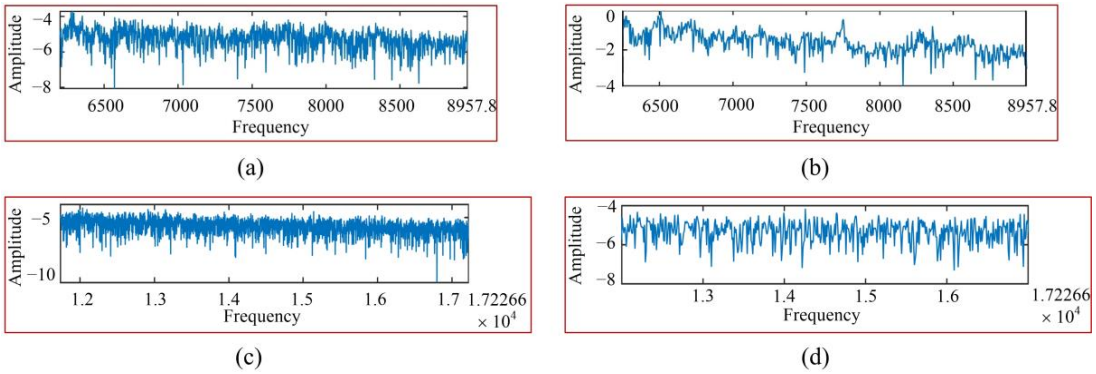


Figure 11. (**a**) Middle-frequency spectrogram of the original signal (6.2016-8.9578 kHz); (**b**) Middle-frequency spectrum of the denoised signal (6.2016-8.9578 kHz); (**c**) High-frequency spectrogram of the original signal (11.7141-17.2266 kHz); (**d**) High-frequency spectrum of the denoised signal (11.7141-17.2266 kHz).

As can be seen from Figure 9, the original signal had obvious noise components and many burrs. However, the improved CEEMDAN denoising method significantly reduced the noise component of the reconstructed signal and retained the original coal–rock cutting sound signal to the maximum extent. As can be seen from Figure 10, the frequency components of the signal were distributed in the whole frequency range [0–22.05 KHz], and the signal spectrum had strong divergence and extremely dense frequency. It has an influence on feature extraction and cutting state recognition of shearer. After denoising, the frequency of background noise was obviously reduced and some wave peaks appeared. At the same time, the signal amplitude decreased after denoising, which was due to the range mutation caused by the removal of noise components. As can be seen from Figure 11, the original signal frequency had strong divergence, frequency density, and chaotic distribution in the mid-to-high-frequency interval of the main distribution of the shearer coal–rock cutting sound signal. Compared with the original signal, the divergence of the signal after denoising was weakened, the frequency of the background noise was obviously reduced, and a more obvious wave peak appeared. The working state of the shearer can be identified according to the wave peak. It showed that the improved CEEMDAN denoising algorithm retained significant advantages in engineering signal processing.

6. Conclusions and Future Work

An adaptive denoising method based on improved CEEMDAN for shearer coal and rock cutting sound signals is proposed in this study. The scouting bee mutation method was combined with FOA, and an adaptive dynamic adjustment search strategy was introduced to avoid falling into the local extremum, improve the convergence accuracy, and maintain the convergence speed based on basic FOA. After CEEMDAN decomposition of the coal–rock cutting sound signal containing noise, the highest SNR of the reconstructed signal was taken as the objective function, and IFOA was used to find the optimal threshold of each order of IMF adaptively through an iterative process to obtain the best denoising effect. The simulation results show that compared with EMD denoising, CEEMDAN denoising, CEEMDAN-PSO denoising, and CEEMDAN-FOA denoising, the SNR_{out} and MSE of the proposed algorithm were improved in different input noise environments. It showed that the algorithm has obvious advantages in denoising under different input noise environments. In the denoising experiment of the shearer coal–rock cutting sound signal, it was found that the noise component of the signal in the time domain diagram and the noise frequency in the frequency spectrum diagram were significantly reduced. In addition, the frequency domain diagram shows a wave peak that determines the working state. The method's effectiveness in practical applications was proved.

However, this method also has some shortcomings and drawbacks, which can be listed as follows: On the one hand, although the proposed improved CEEMDAN denoising method is more effective than other denoising methods, the computational time is still a serious problem that cannot be ignored. On the other hand, the parameters in the optimization process are determined based on previous scholars and a large number of simulation experiments and lack a rigorous mathematical derivation. Several improvements to the proposed method are planned for the future. These may include an improved algorithm code with higher execution efficiency and an appropriate scheme for determining the optimization parameters.

Author Contributions: J.X. (Jing Xu) and C.R. contributed the new method; J.X. (Jie Xu), C.R., Y.L. and N.S. designed the simulations and experiments; J.X. (Jie Xu) and C.R. performed the experiments; C.R. wrote the paper. All authors have read and agreed to the published version of the manuscript.

Funding: This research was funded by the National Natural Science Foundation of China (No.51905229), Natural Science Foundation of Jiangsu Province (No. BK20190968), China Postdoctoral Science Foundation (No.2019M661975), Natural Science Foundation for Colleges and Universities of Jiangsu Province (No.19KJB460015) and Marine Equipment and Technology Institute of Jiangsu University of Science and Technology (HZ20220001). And the APC was funded by Marine Equipment and Technology Institute of Jiangsu University of Science and Technology (HZ20220001).

Institutional Review Board Statement: Not applicable.

Informed Consent Statement: Not applicable.

Data Availability Statement: Not applicable.

Acknowledgments: The author thanks the National Energy Mining Equipment Research Experimental Center of China Coal Zhangjiakou Coal Mining Machinery Co., Ltd. and all the staff for their experimental support.

Conflicts of Interest: The authors declare no conflict of interest.

References

1. Si, L.; Wang, Z.B.; Jiang, G. Fusion recognition of shearer coal-rock cutting state based on improved RBF neural network and DS evidence theory. *IEEE Access* **2019**, *7*, 122106–122121. [CrossRef]
2. Li, C.; Peng, T.; Zhu, Y. A novel approach for acoustic signal processing of a drum shearer based on improved variational mode decomposition and cluster analysis. *Sensors* **2020**, *20*, 2949. [CrossRef] [PubMed]
3. Peng, T.; Li, C.; Zhu, Y. Design and Application of Simulating Cutting Experiment System for Drum Shearer. *Appl. Sci.* **2021**, *11*, 5917. [CrossRef]
4. Li, C.; Peng, T.; Zhu, Y. A Cutting Pattern Recognition Method for Shearers Based on ICEEMDAN and Improved Grey Wolf Optimizer Algorithm-Optimized SVM. *Appl. Sci.* **2021**, *11*, 9081. [CrossRef]
5. Rhif, M.; Abbes, A.B.; Farah, I.; Martínez, B.; Sang, Y.F. Wavelet Transform Application for/in Non-Stationary Time-Series Analysis: A Review. *Appl. Sci.* **2019**, *9*, 1345. [CrossRef]
6. Chen, Z. Signal Recognition for English Speech Translation Based on Improved Wavelet Denoising Method. *Adv. Math. Phys.* **2021**, *2021*, 6811192. [CrossRef]
7. Barbosh, M.; Singh, P.; Sadhu, A. Empirical mode decomposition and its variants: A review with applications in structural health monitoring. *Smart Mater. Struct.* **2020**, *29*, 093001. [CrossRef]
8. Torres, M.E.; Colominas, M.A.; Schlotthauer, G.; Flandrin, P. A complete ensemble empirical mode decomposition with adaptive noise. In Proceedings of the 36th IEEE International Conference on Acoustics, Speech, and Signal Processing (ICASSP'11), Prague, Czech Republic, 22–27 May 2011; pp. 4144–4147.
9. Zheng, Y.; Li, S.; Xing, K. A Novel Noise Reduction Method of UAV Magnetic Survey Data Based on CEEMDAN, Per-mutation Entropy, Correlation Coefficient and Wavelet Threshold Denoising. *Entropy* **2021**, *23*, 1309. [CrossRef]
10. Peng, Y.; Liu, Y.; Zhang, C.; Li, W. A Novel Denoising model of underwater drilling and blasting vibration signal based on CEEMDAN. *Arab J. Sci. Eng.* **2021**, *46*, 4857–4865. [CrossRef]
11. Zhang, S.; Liu, H.; Hu, M. An adaptive CEEMDAN thresholding denoising method optimized by nonlocal means algorithm. *IEEE Trans. Instrum. Meas.* **2020**, *69*, 6891–6903. [CrossRef]
12. Dang, S.W.; Li, L.J.; Wang, Q.Q.; Le, W.K.; Cheng, P.Z. Fiber optic gyro noise reduction based on hybrid CEEMDAN-LWT method. *Measurement* **2020**, *161*, 107865.
13. Li, Y.; Wang, L. A novel noise reduction technique for underwater acoustic signals based on complete ensemble empirical mode decomposition with adaptive noise, minimum mean square variance criterion and least mean square adaptive filter. *Def. Technol.* **2020**, *16*, 543–554. [CrossRef]
14. Cai, J.H.; Xiao, Y.L. Impulse interference processing for MT data based on a new adaptive wavelet threshold de-noising method. *Arab. J. Geosci.* **2017**, *10*, 407.
15. Gao, L.; Gan, Y.; Shi, J. A novel intelligent denoising method of ECG signals based on wavelet adaptive threshold and mathematical morphology. *Appl. Intell.* **2022**, *6*, 1–15. [CrossRef]
16. Zhang, Y.; Chen, Y. Application of hybrid model based on CEEMDAN, SVD, PSO to wind energy prediction. *Environ. Sci. Pollut. Res.* **2021**, *5*, 1–14. [CrossRef] [PubMed]
17. Pan, W.T. A new fruit fly optimization algorithm: Taking the financial distress model as an example. *Knowl. Based Syst.* **2012**, *26*, 69–74. [CrossRef]
18. Pun, P.; Brown, J.; Cobb, T. Navigation of a Freely Walking Fruit Fly in Infinite Space Using a Transparent Omnidirectional Locomotion Compensator (TOLC). *Sensors* **2021**, *21*, 1651. [CrossRef]
19. Peng, L.; Zhu, Q.; Lv, S.X.; Wang, L. Effective long short-term memory with fruit fly optimization algorithm for time series forecasting. *Appl. Soft Comput.* **2020**, *24*, 15059–15079. [CrossRef]

20. Qiao, L.; Liu, Y.; Zhu, J. Application of generalized regression neural network optimized by fruit fly optimization algorithm for fracture toughness in a pearlitic steel. *Eng. Fract. Mech.* **2020**, *235*, 107105. [CrossRef]
21. Luo, R.; Zheng, H.; Guo, J. Solving the multi-functional heterogeneous UAV cooperative mission planning problem using multi-swarm fruit fly optimization algorithm. *Sensors* **2020**, *20*, 5026. [CrossRef]
22. Li, Z.; Qin, Y.; Hou, S. Renewable energy system based on IFOA-BP neural network load forecast. *Energy Rep.* **2020**, *6*, 1585–1590. [CrossRef]
23. Guo, C.; Shang, W. Tourist demand prediction model based on improved fruit fly algorithm. *Secur. Commun. Netw.* **2021**, *2021*, 3411797. [CrossRef]
24. Shi, J.; Mao, Y.; Li, P.; Liu, G.P.; Liu, P.; Yang, X.Y.; Wang, D.H. Hybrid mutation fruit fly optimization algorithm for solving the inverse kinematics of a redundant robot manipulator. *Math. Probl. Eng.* **2020**, *2020*, 6315675. [CrossRef]
25. Zhang, S.; Li, Y. Seismic exploration desert noise suppression based on complete ensemble empirical mode decomposition with adaptive noise. *J. Appl. Geophys.* **2020**, *180*, 104055. [CrossRef]
26. Li, G.; Yang, Z.; Yang, H. A denoising method of ship radiated noise signal based on modified CEEMDAN, dispersion entropy, and interval thresholding. *Electronics* **2019**, *8*, 597. [CrossRef]
27. Chang, J.; Zhu, L.; Li, H.; Xu, F.; Liu, B.G.; Yang, Z.B. Noise reduction in Lidar signal using correlation-based EMD combined with soft thresholding and roughness penalty. *Opt. Commun.* **2018**, *407*, 290–295. [CrossRef]
28. Xie, B.; Xiong, Z.; Wang, Z.; Zhang, L.J.; Zang, L.J.; Li, F.S. Gamma spectrum denoising method based on improved wavelet threshold. *Nucl. Eng. Technol.* **2020**, *52*, 1771–1776. [CrossRef]
29. Fan, S.; Wang, X.; Zhang, Y. Study on PD detection for GIS based on autocorrelation coefficient and similar Wavelet soft threshold. *Clust. Comput.* **2019**, *22*, 6755–6766. [CrossRef]
30. Xu, J.; Wang, Z.; Tan, C.; Si, L.; Zhang, L.; Liu, X.H. Adaptive wavelet threshold denoising method for machinery sound based on improved fruit fly optimization algorithm. *Appl. Sci.* **2016**, *6*, 199. [CrossRef]
31. Sato, J.; Yamada, T.; Ito, K. Artificial Bee Colony for Affine and Perspective Template Matching. *IEEJ T Electr. Electron.* **2022**, *17*, 566–574. [CrossRef]
32. Chen, M. Improved artificial bee colony algorithm based on escaped foraging strategy. *Chin. J. Androl.* **2019**, *42*, 516–524. [CrossRef]
33. Ma, B.; Zhang, T. Single-channel blind source separation for vibration signals based on TVF-EMD and improved SCA. *IET Image Process.* **2020**, *14*, 259–268. [CrossRef]
34. Lou, S.T.; Zhang, X.D. Fuzzy-based learning rate determination for blind source separation. *IEEE Trans. Fuzzy Syst.* **2003**, *11*, 375–383.
35. Liu, Y.; Mu, Y.; Chen, K. Daily activity feature selection in smart homes based on pearson correlation coefficient. *Neurosci. Lett.* **2020**, *51*, 1771–1787. [CrossRef]
36. Si, W.; Qin, B.; Li, Q.; Liu, S.H. A novel adaptive wavelet threshold estimation based on hybrid particle swarm optimization for partial discharge signal denoising. *Optik* **2019**, *181*, 175–184. [CrossRef]
37. Yang, G.; Dai, J.; Liu, X.; Wu, X.L.; Chen, M.; Qin, H. Denoising of gamma-ray spectrum by optimized wavelet thresholding based on modified genetic algorithm in carbon/oxygen logging. *J. Radioanal. Nucl. Chem.* **2019**, *320*, 351–359. [CrossRef]
38. Chen, W.; Li, J.; Wang, Q.; Han, K. Fault feature extraction and diagnosis of rolling bearings based on wavelet thresholding denoising with CEEMDAN energy entropy and PSO-LSSVM. *Measurement* **2021**, *172*, 108901. [CrossRef]